Hugoniot Data for Helium in the Ionization Regime

J. Eggert,[1] S. Brygoo,[1,2] P. Loubeyre,[2] R. S. McWilliams,[1,3] P. M. Celliers,[1] D. G. Hicks,[1] T. R. Boehly,[4] R. Jeanloz,[3] and G. W. Collins[1]

[1]*Lawrence Livermore National Laboratory, Livermore, California 94551, USA*
[2]*Departement de Physique, Théorique et Applications, CEA, Commissariat à l'Energie Atomique, 91680 Bruyères-le-Châtel, France*
[3]*University of California, Berkeley, California, USA*
[4]*Laboratory for Laser Energetics, University of Rochester, Rochester, New York, USA*

(Received 25 August 2007; published 28 March 2008)

Hugoniot data were obtained for fluid He in the 100 GPa pressure range by shock compression of samples statically precompressed in diamond-anvil cells. The initial (precompressed) He density (ρ_1) for each experiment was tuned to a value between $\rho_{0L} < \rho_1 < 3.3\rho_{0L}$, where ρ_{0L} is the zero-pressure density of the cryogenic liquid ($\rho_{0L} = 0.123$ g/cm^3). The maximum observed shock-compression ratios range from $\rho/\rho_1 = 6$ for $\rho_1 = \rho_{0L}$ to $\rho/\rho_1 = 4$ for $\rho_1 \geq 3\rho_{0L}$ (i.e., $\rho/\rho_{0L} \geq 12$). Data show an increase in compressibility at the onset of ionization, similar to theoretical predictions.

DOI: 10.1103/PhysRevLett.100.124503 PACS numbers: 51.30.+i, 52.25.Kn, 62.50.−p, 64.30.−t

The properties of dense He at thermodynamic conditions between those of condensed matter and high-temperature plasmas are theoretically challenging and critical to understanding the evolution and internal structure of Jupiter, Saturn, and extrasolar giant planets [1–6]. To date, the only He equation of state (EOS) data in this regime are the Hugoniot data of Nellis *et al.* [7]. Those experiments used cryogenic techniques to achieve initial densities in the liquid state of $\rho_{0L} = 0.123$ g/cc, and they reached final state pressures of 16 GPa and 56 GPa with single and double shocks, respectively [7]. The EOS currently used by the astrophysical community from Saumon *et al.* (SCVH), which is a free energy based ''chemical'' model, has been calibrated to these few data [8]. The SCVH, path-integral Monte Carlo (PIMC) [2] calculations and activity expansion (ACTEX) calculations of the He Hugoniot all predict an increase in compressibility at the onset of ionization. For an initial density of $\rho_1 = \rho_{0L}$, PIMC calculations predict a maximum single-shock compression $\eta^{\max} = (\rho/\rho_1)^{\max} = 5.3$ near 360 GPa, whereas the SCVH and ACTEX predict $\eta^{\max} \sim 6$ at 300 GPa and 100 GPa, respectively. Thus, Hugoniot data in the 100 GPa range should provide an important test for theoretical descriptions of partially ionized dense fluid He.

Presented here are the first Hugoniot data for He exceeding 100 GPa. Shock data were obtained at several different initial He densities, ranging from the cryogenic liquid $\rho_{0L} = 0.123$ g/cm^3 to $3.3\rho_{0L}$, by combining laser-shock and static-compression techniques [9]. This combination is analogous to multiple-shock compression, allowing significantly higher densities to be achieved because shock-induced heating is reduced. Quartz was used as a reference material allowing shock velocities to be determined just before and just after the shock crosses the quartz-He interface. This significantly reduced the measurement uncertainty as compared to previous studies [9,10].

Experiments were conducted on the Omega laser facility, with drive energies up to 3 kJ and a pulse length of 1 ns [11]. Phase plates in each beam produced a flattop-intensity profile of 650 or 800 μm diameter for generation of planar shocks. A sketch of the precompressed laser-shock targets is shown in Fig. 1(a), together with the orientation of the VISAR (velocity interferometer system for any reflector) diagnostic which measured shock or interface velocities [12]. The drive side of the thin (100 to 250 μm thick) diamond was typically coated with an x-ray preheat shield (2 μm Au) and a plastic ablator. On the sample chamber side, the thin diamond was flash coated with 1000 angstroms of Al, and a quartz plate and a small ruby ball were placed on it. The sapphire anvil and quartz plate have antireflection coatings so that the VISAR does not detect spurious reflections from the stationary interfaces during the experiment. The target was loaded with He in a high-pressure vessel [13].

Determining shock velocities in the quartz standard (U_s^Q) and in He (U_s^{He}) as well as the initial pressure-density-internal energy conditions in the precompressed sample, P_1, ρ_1, and E_1 are essential to determining the P, ρ, and E of the shock-compressed state through the Rankine-Hugoniot equations. P_1 was measured using the ruby-fluorescence method [14], taking into account the temperature shift of the frequency to achieve an absolute precision of ± 0.025 GPa. The precompressed values of ρ_1 and E_1 were then derived from an accurate EOS for fluid He [13]. He samples were precompressed to pressures ranging from 0.11 GPa ($\rho_1 = 0.122$ g/cm^3) to 1.25 GPa ($\rho_1 = 0.429$ g/cm^3). The preshot thicknesses of He and quartz were accurately determined by interferometry and the known refractive indexes of He [15] and quartz [16,17]. The thickness of the quartz plate and He were about 25 μm and 100 μm, respectively.

The line imaging VISAR diagnostic [12] was used to characterize the kinematic and optical parameters of

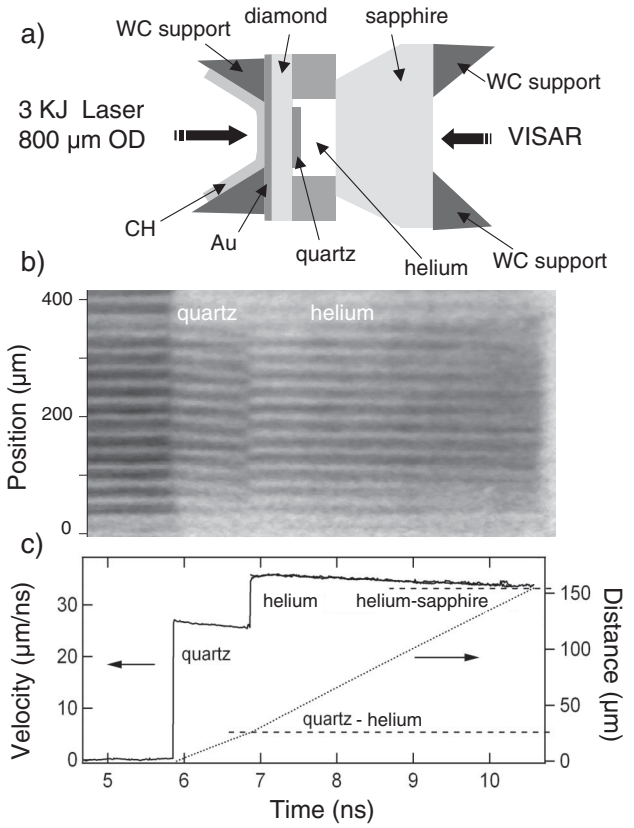

FIG. 1. (a) Sketch of a precompressed target. (b) Example VISAR record obtained from precompressed He ($\rho_1 = 0.122$ g/cc, shocked to 117 GPa). The shock front in both quartz and in He are reflecting. Before 5.9 ns, fringes are produced by reflection of the probe beam from the stationary Al coating between the thin diamond and quartz plate. At ~5.9 ns, the shock enters the quartz and the shock front in the quartz is reflecting. At 6.9 ns, the shock front enters the He and again the shock is so strong, He is reflecting. The shock then passes through the He and enters the back anvil at 10.6 ns. (c) Shock velocity (left scale) and shock trajectory (right scale) in both the quartz and He. The dotted lines represent the quartz and He thicknesses (right scale) measured before the shock experiment. The calculated thickness obtained from shock trajectory agrees to within 2% with the quartz and He thicknesses determined before the shot.

shock-compressed He. At the highest P studied here, shock-compressed He transforms to an electronically conductive state and the shock front reflects the 532 nm probe laser beam of the VISAR diagnostic; U_s^{He} was thus measured both directly from the VISAR fringe shift, as well as from the transit-time of the shock across the known thickness of He. Shocked quartz was reflecting for all of the experiments reported here, so again U_s^Q was determined both directly from the VISAR fringe shift and the shock-transit time. This technique has been validated previously on several materials including quartz [18].

Figure 1(b) shows the fringe pattern for a reflective shock in He. The Doppler shift of the light reflected from the shock front is manifested as a fringe shift at the image output of the velocity interferometer. A velocity accuracy ~1% can be achieved because the fringe position is determined to ~5% of a fringe and the shock velocities measured here correspond typically to 5–7 fringes. To resolve fringe jump ambiguities, data were collected simultaneously from two independent interferometers with different sensitivities [12]. The velocity per fringe in the VISAR measurement was corrected for the density dependent refractive index [12,15]. In Fig. 1(b), the shock front is observed first entering the quartz, then breaks out of the quartz plate into precompressed He, and finally enters the back sapphire anvil which is opaque under these shock-loading conditions. Shock planarity was observed to extend over 400 μm, and shock unsteadiness was quantified as a 3% velocity decrease during transit across the quartz plate and He [Fig. 1(c)].

In all cases, the transit distance in both the quartz and He determined from the time-integrated VISAR velocity agrees to within 2% with the thicknesses measured by interferometry before the shock experiment [Fig. 1(c)]. This validates that the shock front in He (and quartz) is indeed reflecting at 532 nm. In some of the experiments, however, shock-compressed He became opaque and non-reflecting. In those cases, U_s^{He} was determined by transit-time measurements only, taking into account the 3% decay in velocity. The error in the velocity measurement was then larger and arose from the ± 1 μm uncertainty in the thickness measurement of He and from the 50 ps uncertainty in the breakout time at the interfaces. Some shots led to the observation of transparent shocked He, for a particle velocity in He, $U_p < 13$ km/s, but accurate values of U_s^{He} could no longer be obtained and the results of those experiments are not presented here. Finally, a 1D hydrodynamic-radiative simulation was performed to quantify the level of preheat in quartz and He. For the maximum laser irradiation intensity used, preheat in quartz was estimated to be 0.06 eV in the quartz and less than 0.02 eV in He. In addition, no motion of the quartz-He interface was observed before shock breakout so preheat can therefore be neglected.

U_s^Q and U_s^{He} are direct experimental observables, and U_s^Q versus U_s^{He} data lie along a single trend with no obvious dependence on ρ_1 (Fig. 2, inset). U_p^{He} is determined by impedance matching [19,20]. The resulting $U_s^{He} - U_p^{He}$ corresponding to 11 different shots define nearly parallel trends where the offset depends on the precompression (Fig. 2). The error bars in U_s^{He} correspond to the VISAR fringe measurements for reflecting shocks and to transit-time and thickness measurements when He was opaque. The error bars in U_p^{He} come from the propagation of the uncertainty in U_s^Q, U_s^{He}, and ρ_0^{He} in the impedance matching construction. The systematic uncertainty from using a quartz reference averages <25% of the random uncertainty shown in Fig. 2 [19–24].

Previous principal Hugoniot data [7] define a steeper slope, $S = \Delta U_s/\Delta U_p$, at lower U_s and U_p, than is found

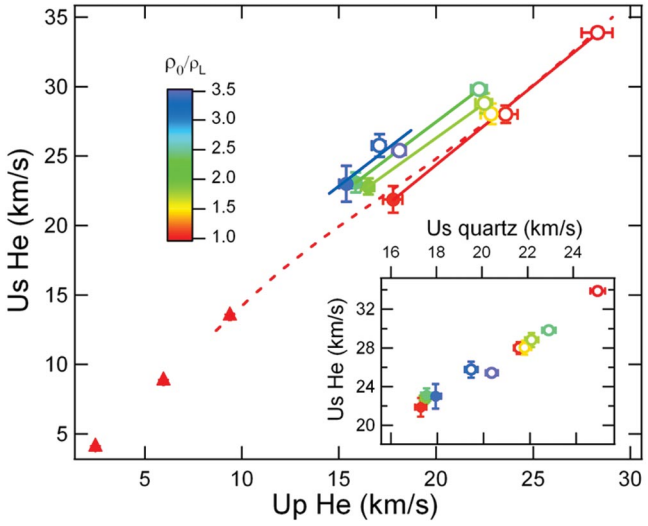

FIG. 2 (color). He shock-wave velocity U_s^{He} vs particle velocity U_p^{He} determined from the experimentally measured values of U_s^{He} and U_s^{Q} (inset). Open and closed symbols indicate whether the shocked state is reflecting or opaque, respectively, with the color showing the initial density, ρ_1, relative to the liquid density, ρ_{0L}. Previous gas-gun data [7] ($\rho_1 = \rho_{0L} = 0.1233$ g/cc) are plotted as triangles, and the dashed curve shows the results of ACTEX calculations [3].

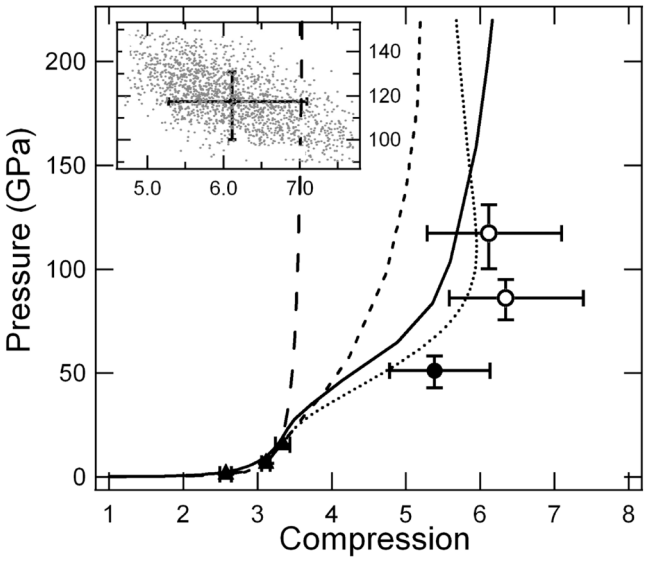

FIG. 3. (a) Hugoniot data for an initial density $\rho_1 = 0.123$ g/cc, i.e., of cryogenic He and of He precompressed at 0.12 GPa at room temperature. The symbols are the same as in Fig. 2. Also shown are the gas-gun data from Nellis *et al.* [7] with $\rho_1 = 0.123$ g/cc (▲) and model calculations from SCVH [8] (solid line), ACTEX [3] (dotted line), and DFT/PIMC [2] (short dashed line). To compare these new data to the expected Hugoniot without electronic excitations, the lower pressure gas-gun data are extrapolated assuming a linear U_s vs U_p (long dashed line). Inset shows the estimation of the 1-sigma error bars from a Monte Carlo calculation for the highest pressure datum.

for the present measurements at higher pressure (Fig. 2). A decrease in S has typically been observed for metals at high shock P, where it is ascribed to electronic excitations [21]. Similarly, the difference in S for the present experiments occurs as the shocked He transitions from transparent to reflecting, indicating a significant increase in electron-carrier concentration. The actual Hugoniot in $U_s - U_p$ is expected to smoothly transition to a smaller slope similar to the dashed line in Fig. 2 which represents the theoretical Actex calculation [3]. At higher P than those studied here, He will become more fully ionized, and S should increase back to a value close to that observed at lower P. The offsets in $U_s(U_p)$ lines are largely due to the difference in the initial sound speed for He due to the different initial densities.

The P, ρ values of shocked He are determined from U_s^{He} and U_p^{He} using the Rankine-Hugoniot relations: $P = \rho_1 U_s U_p$ and $\rho = \rho_1 U_s/(U_s - U_p)$, where ρ_1 is the initial density [25]. P versus $\eta = \rho/\rho_1$ data for samples starting at the cryogenic-liquid density, $\rho_1 = \rho_{0L} = 0.123$ g/cc, are shown in Fig. 3, along with the prior data [7]. Error bars are estimated with a Monte Carlo algorithm from an assumed Gaussian distribution about each observable, U_s^{He}, U_s^{Q}, and P_1 (inset to Fig. 3). At low precompression, the random uncertainty is largely determined by the uncertainty in P_1 (± 0.025 GPa precision of the ruby scale) and hence in ρ_1. At higher precompression, the uncertainty in P_1 gives a smaller contribution to the density uncertainty (see Fig. 4).

The new data presented here for $\rho_1 = \rho_{0L}$ extend previous gas-gun data by more than 5 times in P, up to 120 GPa, and reveal $\eta \sim 6$ at $\sim$100 GPa. This is in good agreement with the two chemical models, SCVH [8] and ACTEX [3], and it shows the *ab initio* calculation [2] underestimates η. Moreover, a Hugoniot curve extrapolated from the lower-P gas-gun data assuming a linear $U_s - U_p$ relation—which would therefore represent He with no electronic excitations—is seen in Fig. 3 to increase smoothly to a limiting compression of 4, much stiffer than observed here. Thus, these experiments suggest that electronic excitation (ionization) of He can cause an increase in η of $\sim$50% along the principal Hugoniot.

Increasing ρ_1 enables EOS measurements at higher ρ than can be achieved along the principal Hugoniot. Importantly, these higher ρ actually correspond to lower η, as shown in Fig. 4. The reason for this arises from the fact that $\eta = \rho/\rho_1$ is sensitive to the relative importance of excitations of internal degrees of freedom (which tend to cause higher compressions) as compared to interaction effects (which increase the pressure and thus cause lower compressions) [2]. For the case of He, the lower temperatures accompanying higher ρ_1 result in reduced thermal ionization which, along with the increased interaction effects at higher density, result in a lower η. Figure 4 also shows that at a given pressure the observed change in η with ρ_1 is larger than is predicted by the *ab initio* calculations and the SCVH model. This suggests that

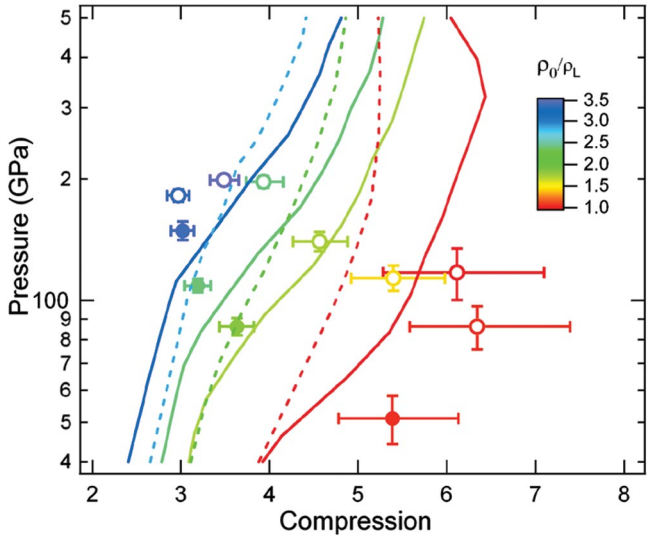

FIG. 4 (color). He Hugoniots for different ρ_1 from $\rho_1 = \rho_{0L}$ to $\rho_1 = 3.3\rho_{0L}$. ○ are the present data. The full line is the SCVH model [8] and the dashed line the *ab initio* calculations [2]. The color and symbol notation for the data is the same as in Fig. 2.

the isentropic compressibility (sound speed) for dense He is lower (higher) than in those predictions. It is also predicted by the SCVH and the *ab initio* calculations that $\eta^{\max}$ on the Hugoniot should decrease with ρ_1. While this expectation is consistent with these new measurements, experiments need to be extended to higher P to fully test this prediction.

In summary, by applying laser-driven shocks to statically compressed samples, EOS data for fluid He have been obtained with sufficient accuracy in the 100 GPa pressure range to test theoretical predictions. Experimental data are listed in Ref. [26]. Tuning ρ_1 before shock loading enables the measurement of a family of Hugoniots, which can test EOS models over a broader range than the principal Hugoniot alone, and can separate the effects of T and ρ on the EOS. The SCVH model used for astrophysical applications reproduces the present data quite well, agreeing with the observed maximum shock-compression ratio of about sixfold (for $\rho_1 = \rho_{0L}$). Extension of the techniques described here to laser drivers capable of depositing >10 kJ onto the sample and with pulse durations longer than 10 ns will significantly increase the accessible P and ρ range with improved accuracy, to provide further discrimination among theoretical approaches currently being used.

We thank the Omega operations staff for their invaluable assistance. We thank M. Millerioux (CEA) for doing the diamond coating and W. Unites (LLNL) for preparing the quartz plates.

[1] V. E. Fortov *et al.*, JETP **97**, 259 (2003).
[2] B. Militzer, Phys. Rev. Lett. **97**, 175501 (2006).
[3] M. Ross, F. Rogers, N. Winter, and G. Collins, Phys. Rev. B **76**, 020502(R) (2007).
[4] C. Winisdoerffer and G. Chabrier. Phys. Rev. E **71**, 026402 (2005).
[5] S. Mazevet, M. Challacombe, P. M. Kowalski, and D. Saumon, Astrophys. Space Sci. **307**, 273 (2007).
[6] D. Saumon and T. Guillot, Astrophys. J. **609**, 1170 (2004).
[7] W. J. Nellis *et al.*, Phys. Rev. Lett. **53**, 1248 (1984).
[8] D. Saumon, G. Chabrier and H. M. Van Horn, Astrophys. J. **99**, 713 (1995).
[9] P. Loubeyre *et al.*, High Press. Res. **24**, 25 (2004); R. Jeanloz *et al.*, Proc. Natl. Acad. Sci. U.S.A. **104**, 9172 (2007); K. K. M. Lee *et al.*, AIP Conf. Proc. **620**, 1363 (2002); J. Chem. Phys. **125**, 014701 (2006).
[10] S. Brygoo *et al.*, J. Appl. Phys. (to be published).
[11] T. R. Boehly *et al.*, Opt. Commun. **133**, 495 (1997).
[12] P. M. Celliers *et al.*, Rev. Sci. Instrum. **75**, 4916 (2004).
[13] R. LeToullec, P. Loubeyre, and J. P. Pinceaux, Phys. Rev. B **40**, 2368 (1989).
[14] H. K. Mao, J. Xu, and P. M. Bell, J. Geophys. Res. B **91**, 4673 (1986).
[15] A. Dewaele, J. Eggert, P. Loubeyre, and R. LeToullec, Phys. Rev. B **67**, 094112 (2003).
[16] E. Meister, E. C. Robertson, R. W. Were, and R. Raspet, J. Geophys. Res. **85**, 6461 (1980).
[17] K. Vedam and T. A. Davis, J. Opt. Soc. Am. **57**, 1140 (1967).
[18] D. G. Hicks *et al.*, Phys. Plasmas **12**, 082702 (2005).
[19] P. M. Celliers, G. W. Collins, D. G. Hicks, and J. H. Eggert, J. Appl. Phys. **98**, 113529 (2005).
[20] Impedance matching requires the knowledge of the quartz Hugoniot [21] and its off-Hugoniot states along release isentropes. The effect of precompression changes slightly the initial density and thus the Hugoniot of quartz in a known way [22]. Release isentropes are estimated with a reflected Hugoniot centered on the initial shock state of the standard together with a correction using a Mie-Grüneisen model for quartz fitted to available data [22]. The resultant Grüneisen parameter used was 0.66. In all experiments both the shock and release states for quartz were in the conducting fluid phase [23]. The release isentropes used here are consistent with those calculated from SESAME tables and Ref. [24]. The systematic uncertainty is obtained by comparing the variance of release isentropes from these different models [19].
[21] R. F. Trunin, Phys. Usp. **37**, 1123 (1994).
[22] S. Brygoo, Ph.D. thesis, Ecole Polytechnique, 2006; T. R. Boehly *et al.*, in *Shock Compression of Condensed Matter–2007*, edited by M. Elert, M. D. Furnish, R. Chau, N. Holmes, and J. Nguyen, AIP Conf. Proc. No. 955 (AIP, New York, 2007).
[23] D. G. Hicks *et al.*, Phys. Rev. Lett. **97**, 025502 (2006).
[24] G. Kerley, "*Equations of State for Composite Materials*," Sandia Technical Report, 2001; Los Alamos National Laboratory Report No. LA-10160-MS.
[25] Y. B. Zeldovich and Y. P. Raizer, *Physics of Shock Waves and High-Temperature Hydrodynamic Phenomena* (Academic, New York, 1967).
[26] See EPAPS Document No. E-PRLTAO-100-032808 for a table of the experimental data. For more information on EPAPS, see http://www.aip.org/pubservs/epaps.html.